

Supplementary material for “Surface flaws control strain localization in the deformation of Cu|Au nanolaminate pillars”

Adrien Gola,^{1,2} Guang-Ping Zhang,³ Lars Pastewka,^{1,2,4,5,*} and Ruth Schwaiger²

¹*Department of Microsystems Engineering, University of Freiburg,
Georges-Köhler-Allee 103, 79110 Freiburg, Germany*

²*Institute for Applied Materials, Karlsruhe Institute of Technology (KIT),
Hermann-von-Helmholtz-Platz 1, 76344 Eggenstein-Leopoldshafen, Germany*

³*Shenyang National Laboratory for Materials Science,
Institute of Metal Research, Chinese Academy of Sciences,
72 Wenhua Road, Shenyang 110016, P.R. China*

⁴*Freiburg Materials Research Center,
University of Freiburg, 79104 Freiburg, Germany*

⁵*Cluster of Excellence livMatS @ FIT – Freiburg Center
for Interactive Materials and Bioinspired Technologies,
University of Freiburg, Georges-Köhler-Allee 105, 79110 Freiburg, Germany*

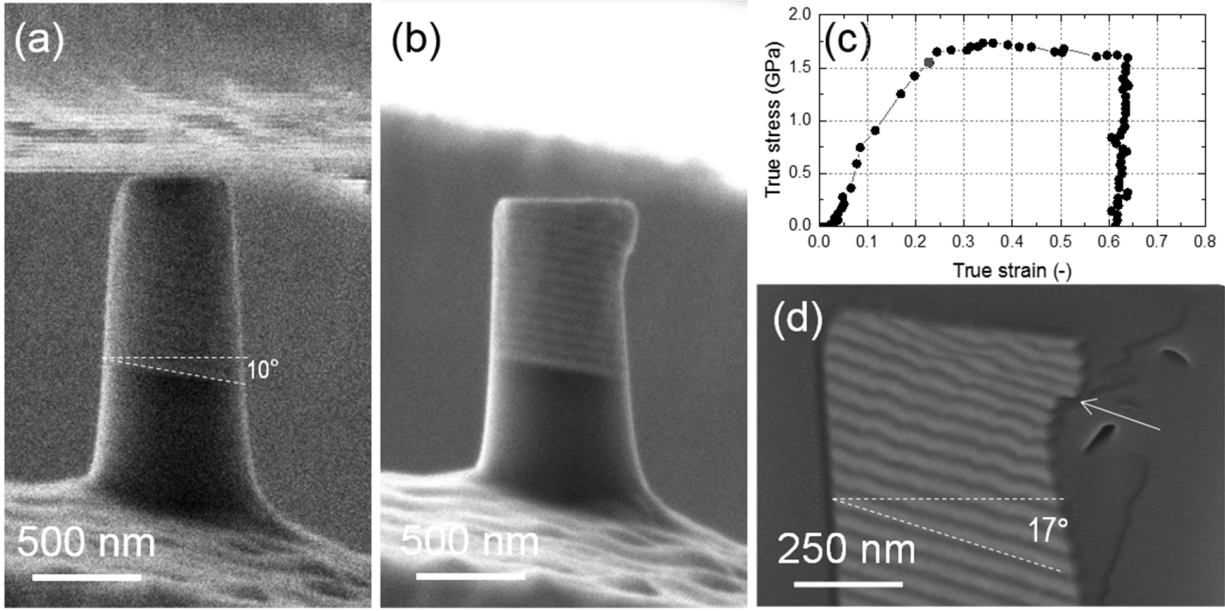


FIG. S-1. (a) SEM image of the 10° tilted pillar prior to deformation. (b) SEM image of the 10° tilted pillar after deformation up to 0.65 strain. (c) True stress - True strain curve obtained for the deformation of the 10° tilted pillar. (d) Post-mortem SEM cross section image of a 17° tilted pillar.

S-I. INTERFACIAL SHEAR STRENGTH

A. Experiment

Pillars with interfaces tilted at an angle of 10° and 17° to the horizontal were prepared by FIB milling. They were deformed in situ in the scanning electron microscope to determine the true stress vs. true strain curves (FEI Nova NanoLab 200 and Nanomechanics InSem nanoindenter). The 10° pillar was deformed to a strain of ≈ 0.65 at the pillar top, where the deformation localized (Fig. S-1). The deformation was stable and shear in the direction of the interface was not observed. At the maximum strain a shear stress acting along the interface of ≈ 0.2 GPa was observed. In case of the 17° pillar, more pronounced steps on the pillar side-face were observed (marked by arrow in Fig. S-1d), while the pillar did not fail catastrophically. The maximum shear stress along the interface was ≈ 0.3 GPa.

B. Simulation

We used representative volume elements to compute the interfacial shear strength of the Cu|Au using molecular dynamic calculations. The system represented in Fig. S-2a was composed of a single bilayer with a layer thickness of 5 nm and periodic boundary conditions in all directions. The system was composed of approximately 200,000 atoms with a box size of approximately $17 \times 19 \times 10 \text{ nm}^3$ along the x , y , and z directions, respectively.

Before straining, the systems was relaxed at 300 K for 500 ps using the Nosé-Hoover/Andersen¹ ensemble without any strain. Simple shear strain was applied along $[112](1\bar{1}\bar{1})$ directions for shear parallel to the nanolaminate interfaces by homogeneously deforming the box. Our notation $[abc](hkl)$ for simple shear reports both the direction of shear $[abc]$ and the plane of shear (hkl) . We used a strain rate of 10^8 s^{-1} in all cases; strain rate dependence of stress is negligible at these rates in FCC metals.² For an atomically sharp interface, the nanolaminate responded to this deformation with a shear stress of a few MPa (Fig. S-2b). This is a clear sign that the system reacted by gliding along the heterointerface. As we probed more realistic systems with Cu and Au intermixed at the interface (see Ref. 3), we observed that the yield stress increased in all the cases to approximately 0.3 – 0.35 GPa. The intermixing width has only a small impact on the yield stress and interfacial shear strength which means that most of the strengthening comes from heterogeneities introduced close the heterointerface. Those act as pinning point for the interfacial dislocation network.⁴

S-II. DETERMINATION OF THE PILLAR CROSS-SECTION

To facilitate comparison with experiments, we evaluated the MD simulations in the same way the experiments were evaluated: Stress $\sigma = F/A$ is computed by dividing the force F on the indenter by the cross-sectional area A at a position 1/5 along the pillar from its top. Since experiments only have access to a side view (Fig. S-1) and must assume rotational symmetry, we investigated the influence of this assumption on the stress-strain curves. MD calculation allows us to access both the exact area and the apparent diameter of a given cross section as shown in Fig. S-1a. We computed the exact area A from the convex hull of the cross section at the given height (red line in Fig. S-3a). We also computed the length of the semi-minor and semi-major axes of the pillar (as shown by the dashed lines in Fig. S-3a). With these

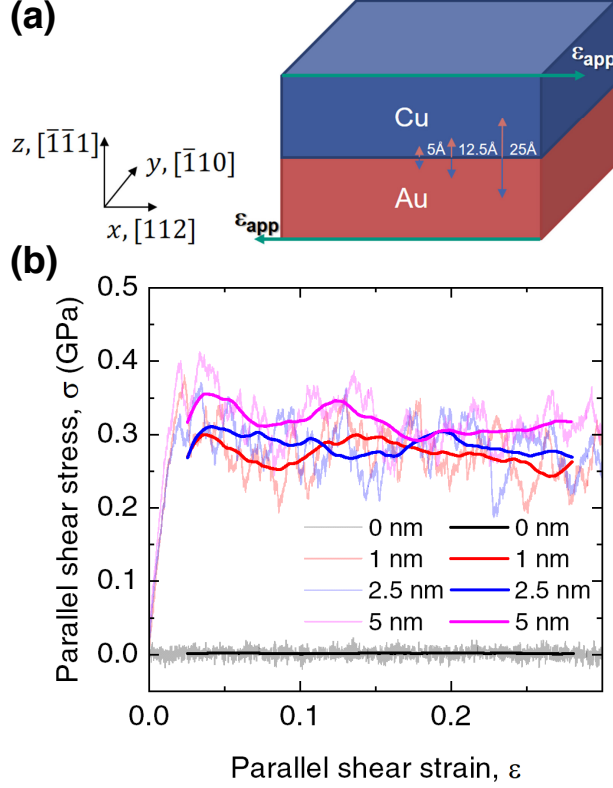


FIG. S-2. (a) Illustration of the Cu|Au nanolaminate simulation geometry and the applied strain direction used for the determination of the interfacial shear strength. (b) Stress-strain curves during simple shear at 300 K parallel to the heterointerface of the Cu|Au nanolaminate system with a layer thickness of 5 nm and intermixing width $w = 0, 1, 2.5$ and 5 nm. Thick lines are moving averages over a strain interval ± 0.025 around the respective data point, thin lines show the full data.

measurements we determined the lateral strain in the pillar, $\epsilon = \ln(1 + (d - d_0)/d_0)$ where d_0 is the initial diameter. Fig. S-3b shows the results obtained for the different definitions of the cross-sectional area A (smallest and largest cross section, exact convex hull) for an exemplary calculation. We observe for all the cases a yield at $\sigma \approx 4$ GPa and ϵ ranging from 0.1% to 1% followed by some strain softening. The maximal lateral strain is achieved for the largest cross-section definition with $\epsilon \approx 25\%$ the smallest cross section reaches $\epsilon \approx 22\%$ and the exact convex hull area $\epsilon \approx 19\%$. In all the cases, the final stress value is around $\sigma \approx 2.3$ GPa. These results show that the assumption made in the experiments does not have a significant influence on the outcome of the stress-strain curves.

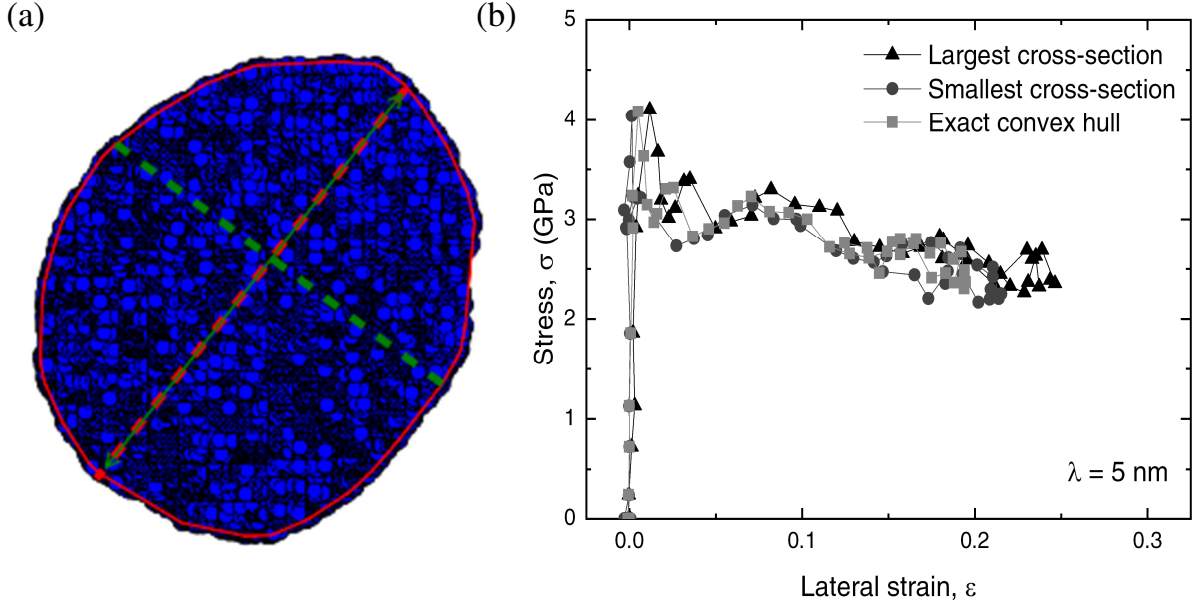


FIG. S-3. (a) Example of a cross section extracted from a pillar during indentation. The set of blue dots show the atom positions, the red solid line displays the convex hull of this given set of points. The red and green dashed lines represent the largest and smallest apparent diameters, respectively. (b) Stress-strain curves of pillar compression for the MD calculation with layer thickness $\lambda = 5$ nm.

S-III. INFLUENCE OF DEFECTS ON THE STRESS-STRAIN CURVES

Consistent with previous observation from calculations of bulk or surface deformation,^{5,6} the defect-free system (Fig. S-4) yielded at a peak stress roughly double the flow stress of the material. The introduction of interface defects reduces this value but only surface defects and bulk defects led to smooth stress-strain curves qualitatively comparable to the one obtained in our experiments.

S-IV. DEFORMATION OF SINGLE-CRYSTALLINE AU PILLARS

We carried out control calculations using single crystal Au pillars of 60 nm height, equal to the total pillar height for the nanolaminate pillars with $\lambda = 5$ nm layer thickness. Fig. S-5 show that the pillar deforms homogeneously even in the presence of a surface step. Alongside the atomic position we also show an analysis of the dislocation structure obtained with the dislocation extraction algorithm (DXA, Ref. 7). We obtain the same results for self-

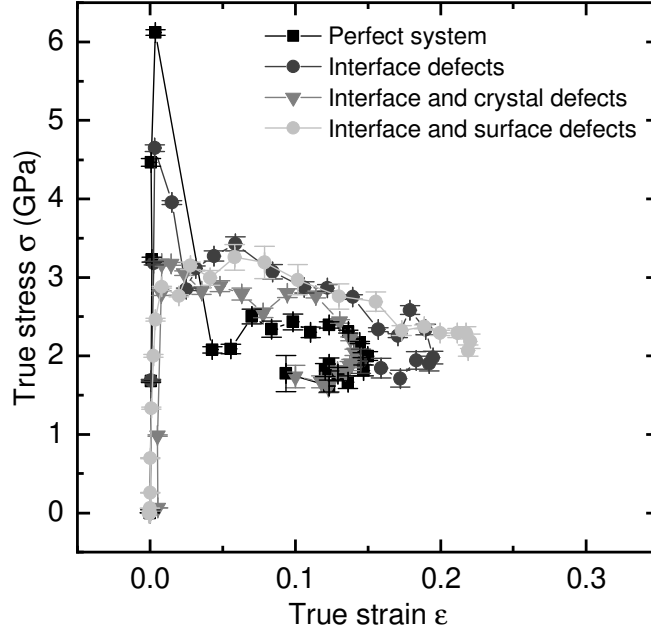


FIG. S-4. Stress-strain curves obtained from MD simulations with controlled defects. The error bars of the simulated data are obtained by repeating the area measurement at distances ≈ 1 nm of the reference cross section.

affine roughness (not shown here). We observed that after a dislocation nucleates at the surface (Fig. S-5b) it crosses the full pillar, vanishing at the sidewall and leaving behind a complementary step (Fig. S-5c-d). Unlike in nanolaminates, this dislocation does not imprint its signature into the bulk of the material. Further compression lead to new dislocations nucleating from the top pillar surface (Fig. S-5e). While some dislocations escape the pillar, others react in the bulk or pile up against the fixed layer at the bottom (Fig. S-5f-i).

* lars.pastewka@imtek.uni-freiburg.de

¹ W. Shinoda, M. Shiga, and M. Mikami, Phys. Rev. B **69**, 134103 (2004).

² M. F. Horstemeyer, M. I. Baskes, and S. J. Plimpton, Acta Mater. **49**, 4363 (2001).

³ A. Gola and L. Pastewka, in *NIC Symposium 2018 - Proceedings*, NIC Series, edited by K. Binder, M. Müller, and A. Trautmann (Forschungszentrum Jülich, Jülich, Germany, 2018) pp. 247–254.

⁴ A. Gola, P. Gumbsch, and L. Pastewka, Acta Mater. **150**, 236 (2018).

⁵ L. A. Zepeda-Ruiz, A. Stukowski, T. Ooppelstrup, and V. V. Bulatov, Nature **550**, 492 (2017).

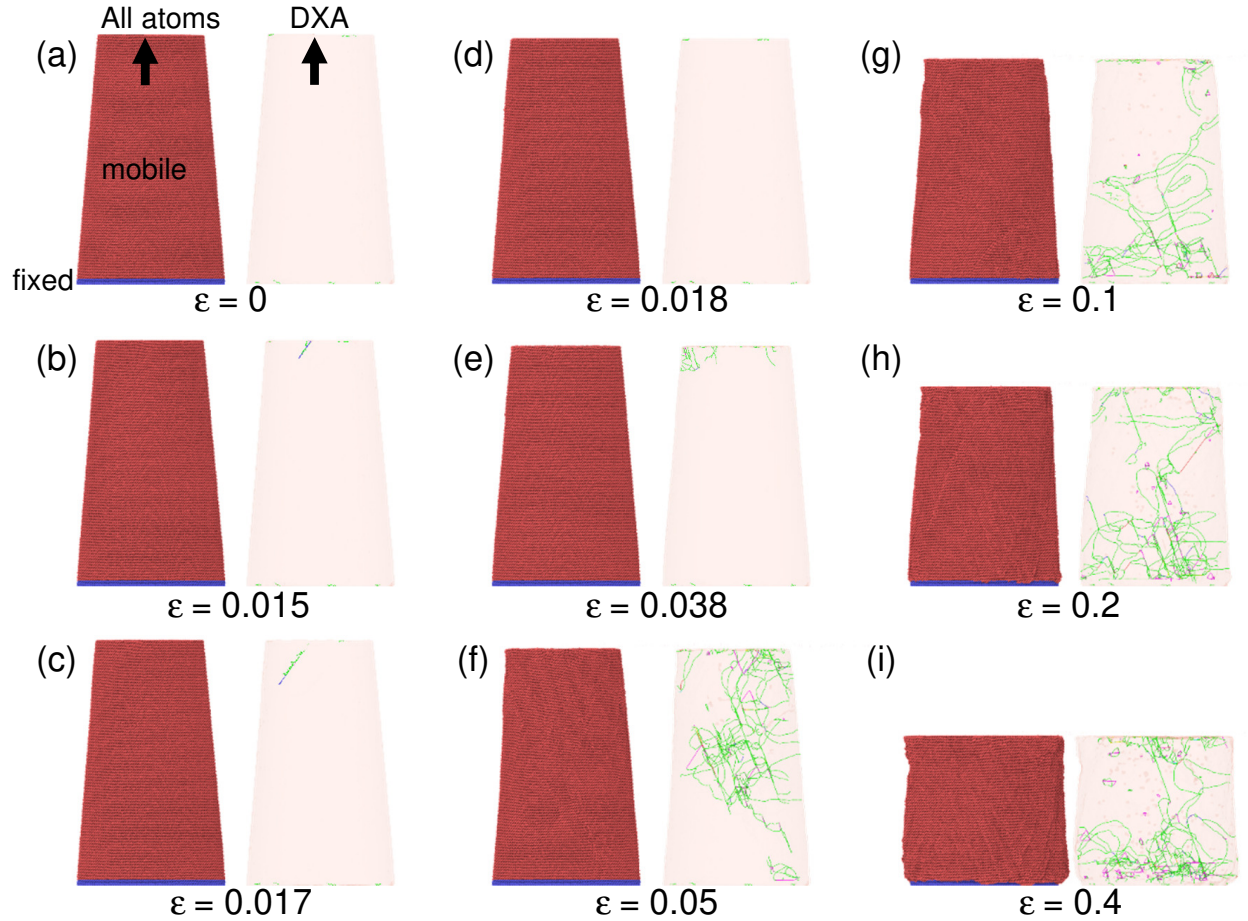


FIG. S-5. Deformation of an Au single crystal nanopillar of 60 nm height under compression. The arrows in (a) mark the location of the single atomic step at the surface. Atoms are color coded after their mobility with red atoms being mobile and blue fixed. We used the dislocation extraction algorithm (DXA) to display the dislocations at each deformation stage. The shaded surface represents the nanopillar surface, Shockley partial dislocations are in green and stair-rod dislocations in purple. The individual panels (a-i) show snapshots of a single calculation at different values of the applied strain ε indicated below the respective figure.

⁶ A. Klemenz, A. Gola, M. Moseler, and L. Pastewka, *Appl. Phys. Lett.* **112**, 061601 (2018).

⁷ A. Stukowski, V. V. Bulatov, and A. Arsenlis, *Model. Simul. Mater. Sci. Eng.* **20**, 085007 (2012).